Non-linear Dynamics Method to Angles-Only Navigation for Non-cooperative Rendezvous of Spacecraft

DU Ronghua, LIAO Wenhe, ZHANG Xiang*

College of Mechanical Engineering, Nanjing University of Science and Technology, Nanjing 210094, P. R. China

(Received 10 January 2022; revised 9 May 2022; accepted 14 July 2022)

Abstract: Aiming at the problem of relative navigation for non-cooperative rendezvous of spacecraft, this paper proposes a new angles-only navigation architecture using non-linear dynamics method. This method does not solve the problem of poor observability of angles-only navigation through orbital or attitude maneuvering, but improves the observability of angles-only navigation through capturing the non-linearity of the system in the evolution of relative motion. First, three relative dynamics models and their corresponding line-of-sight (LoS) measurement equations are introduced, including the rectilinear state relative dynamics model, the curvilinear state relative dynamics model, and the relative orbital elements (ROE) state relative dynamics model. Then, an observability analysis theory based on the Gramian matrix is introduced to determine which relative dynamics model could maximize the observability of angles-only navigation. Next, an adaptive extended Kalman filtering scheme is proposed to solve the problem that the angles-only navigation filter using the non-linear dynamics method is sensitive to measurement noises. Finally, the performances of the proposed angles-only navigation architecture are tested by means of numerical simulations, which demonstrates that the angles-only navigation filtering scheme without orbital or attitude maneuvering is completely feasible through improving the modeling of the relative dynamics and LoS measurement equations.

Key words: angles-only navigation; non-linear dynamics; observability analysis; non-cooperative rendezvous; adaptive Kalman filter

CLC number: V249.32 **Document code:** A **Article ID:** 1005-1120(2022)04-0400-15

0 Introduction

Angles-only navigation is not a new concept, and it was first used in the 19th century when the scientists observed celestial bodies through telescopes and calculated their orbits. So far, angles-only navigation has been widely used and studied in sailing[1], deep space exploration[2], spacecraft orbit determination[3], and formation flying[4-5].

The concept of angles-only navigation is quite simple. The LoS vectors between the chaser spacecraft and the space target can be measured by a monocular camera over a period of time to determine the relative motion states between them[6]. The active sensors such as light detection and ranging (LiDAR) and microwave radars are commonly used to measure relative motion states between two spacecraft. However, they cannot be applied to micro-satellite platforms due to their high power consumption and large mass. The passive sensors such as optical and infrared cameras have many advantages[7-9] because they are employable at various inter-satellite separation ranges with small effect on the design of the mass/power of the chaser spacecraft[10]. Moreover, most spacecraft are equipped with onboard cameras, if the direction is appropriate, these onboard cameras could be used to capture the space targets within the field of view and perform angles-only navigation operations[11]. This so-called angles-only navigation provides a passive, robust, and high-dynamic-range capability. Accordingly, angles-

*Corresponding author, E-mail address: cnwho@mail.njust.edu.cn.

How to cite this article: DU Ronghua, LIAO Wenhe, ZHANG Xiang. Non-linear dynamics method to angles-only navigation for non-cooperative rendezvous of spacecraft[J]. Transactions of Nanjing University of Aeronautics and Astronautics, 2022, 39(4): 400-414.

http://dx.doi.org/10.16356/j.1005-1120.2022.04.003

only navigation represents a critical enabling technology for a variety of advanced distributed space system missions, including autonomous rendezvous and docking, space situational awareness, advanced distributed aperture science, and on-orbit servicing of non-cooperative spacecraft[12]. In addition, angles-only navigation has great application prospects in space-based anti-missile monitoring and active debris removal[13-14].

Due to the lack of depth information of the monocular camera, angles-only navigation suffers from a relative range observability problem during near-range rendezvous[15-17]. Many scholars have studied the methods to improve the observability of angles-only navigation, including the orbital maneuver method[18], the camera bias method[19], the non-linear dynamics method[20], and the multi-satellite multi-sensor method[21]. The camera bias method is only suitable for close ranges; the orbital maneuver method will increase the fuel cost of the satellite platform; and the multi-satellite multi-sensor method has the disadvantage of complicated hardware configuration.

In view of the problems of the above-mentioned methods, this paper intends to improve the observability of the angles-only navigation system through capturing the non-linearity of the system in the evolution of the relative motion, and an angles-only navigation architecture using non-linear dynamics method is proposed. To solve the problems of angles-only navigation, it is necessary to establish a relative dynamics model and a corresponding LoS measurement equation. First, this paper introduces three spacecraft relative dynamics models, including the rectilinear state relative dynamics model, the curvilinear state relative dynamics model, and the ROE state relative dynamics model. Then, the LoS measurement equation corresponding to each relative dynamics model is established. Second, an observability analysis theory based on the Gramian matrix is introduced to determine which relative dynamics model can maximize the observability of angles-only navigation. Third, an adaptive extended Kalman filtering scheme is proposed to solve the problem that the angles-only navigation filter using non-linear dynamics method is sensitive to the measurement noises. Finally, the performances of the angles-only navigation architecture are tested in a high-fidelity simulation environment, which verifies the effectiveness of the proposed angles-only navigation architecture.

1 Relative Dynamics Models

The relative dynamics model describes how the relative motion states between the chaser spacecraft and the space target evolve over time. In order to meet the requirements of on-board implementation, the relative dynamics model should be simplified as much as possible to save the resources of the on-board computer. The simplified form of the relative dynamics model established in this paper can be expressed as

$$\boldsymbol{x}(t_f)=\boldsymbol{\Phi}(t_f,t_0)\boldsymbol{x}(t_0) \tag{1}$$

where $\boldsymbol{x}(t_0)$ is the relative motion state between the chaser spacecraft and the space target at the initial time t_0; and $\boldsymbol{\Phi}(t_f, t_0)$ the state transition matrix (STM).

Next, three types of relative dynamics models will be introduced, including the rectilinear state relative dynamics model, the curvilinear state relative dynamics model, and the ROE state relative dynamics model.

1.1 Rectilinear state relative dynamics model

For the modeling of the rectilinear state relative dynamics, it is necessary to establish a Cartesian frame with the centroid of the chaser spacecraft as the origin. In this Cartesian frame, the x-axis is aligned with the radial direction (R) of the chaser spacecraft; the y-axis is aligned with the tangential direction (T) of the chaser spacecraft; and the z-axis is aligned with the angular momentum direction (N) of the chaser spacecraft. The rectilinear state vector $\boldsymbol{x}_{\text{rec}}$ includes the rectilinear relative position vector $\boldsymbol{r}_{\text{rec}}$ and the rectilinear relative velocity vector $\boldsymbol{v}_{\text{rec}}$

$$\boldsymbol{x}_{\text{rec}}=(\boldsymbol{r}_{\text{rec}}\quad\boldsymbol{v}_{\text{rec}})^{\text{T}}=\begin{pmatrix}x & y & z & v_x & v_y & v_z\end{pmatrix}^{\text{T}} \tag{2}$$

where x, y, and z represent the rectilinear relative position components in the R, T, and N directions,

respectively; and v_x, v_y, and v_z the rectilinear relative velocity components in the R, T, and N directions, respectively.

For the unperturbed near-circular orbits, the Hill-Clohessy-Wiltshire (HCW) equation can be used to establish the rectilinear state relative dynamics model, and its STM can be given as

$$\boldsymbol{\Phi}(t_f,t_0)=[\boldsymbol{\Phi}_r(t_f,t_0)\quad\boldsymbol{\Phi}_v(t_f,t_0)]=\begin{bmatrix}\boldsymbol{\Phi}_{rr}&\boldsymbol{\Phi}_{rv}\\ \boldsymbol{\Phi}_{vr}&\boldsymbol{\Phi}_{vv}\end{bmatrix} \tag{3}$$

where

$$\boldsymbol{\Phi}_{rr}=\begin{bmatrix}4-3\cos(n\tau)&0&0\\ 6\sin(n\tau)-6n\tau&1&0\\ 0&0&\cos(n\tau)\end{bmatrix} \tag{4}$$

$$\boldsymbol{\Phi}_{rv}=\begin{bmatrix}\dfrac{\sin(n\tau)}{n}&\dfrac{2(1-\cos(n\tau))}{n}&0\\ \dfrac{2(\cos(n\tau)-1)}{n}&\dfrac{4\sin(n\tau)-3n\tau}{n}&0\\ 0&0&\dfrac{\sin(n\tau)}{n}\end{bmatrix} \tag{5}$$

$$\boldsymbol{\Phi}_{vr}=\begin{bmatrix}3\omega\sin(n\tau)&0&0\\ 6n(\cos(n\tau)-1)&0&0\\ 0&0&-n\sin(n\tau)\end{bmatrix} \tag{6}$$

$$\boldsymbol{\Phi}_{vv}=\begin{bmatrix}\cos(n\tau)&2\sin(n\tau)&0\\ -2\sin(n\tau)&4\cos(n\tau)-3&0\\ 0&0&\cos(n\tau)\end{bmatrix} \tag{7}$$

where n is the mean motion of the chaser spacecraft; and $\tau=t_f-t_0$ the time interval.

1.2 Curvilinear state relative dynamics model

In addition to the rectilinear state mentioned above, the curvilinear state can also be used to describe the relative motion states between the chaser spacecraft and the space target, and it can better capture the orbital curvature of the relative motion. The curvilinear state vector $\boldsymbol{x}_{\text{cur}}$ includes the curvilinear relative position vector $\boldsymbol{r}_{\text{cur}}$ and the curvilinear relative velocity vector $\boldsymbol{v}_{\text{cur}}$, where the curvilinear relative position vector $\boldsymbol{r}_{\text{cur}}$ includes the orbital radius difference r, the angular in-plane separation θ, and the angular out-of-plane separation ψ, as shown in Fig.1. For a near-circular orbit, in order to ensure the consistency of dimensions, it is necessary to multiply the angular in-plane separation θ and the angular out-of-plane separation ψ by the orbital semi-major axis a, namely

$$\boldsymbol{x}_{\text{cur}}=(\boldsymbol{r}_{\text{cur}}\quad\boldsymbol{v}_{\text{cur}})^{\mathrm{T}}=\left(r\quad a\theta\quad a\psi\quad\dot{r}\quad a\dot{\theta}\quad a\dot{\psi}\right)^{\mathrm{T}} \tag{8}$$

Fig.1 shows the relationship between the curvilinear state vector $\boldsymbol{x}_{\text{cur}}$ and the absolute position vector $\boldsymbol{\rho}$ of the chaser spacecraft and the space target. Since the first-order curvilinear state and rectilinear state relative dynamics models are the same in the near-circular orbits[22], the STM in Eqs.(3—7) can also be used to propagate the curvilinear relative motion states.

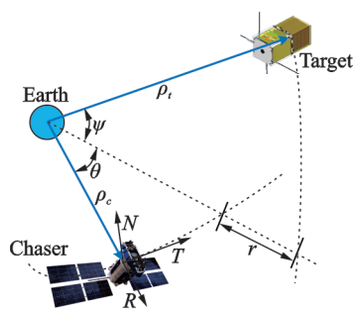

Fig.1 Definition of curvilinear state

1.3 ROE state relative dynamics model

In addition, a set of mean ROE can be used to describe the relative motion states between the chaser spacecraft and the space target. The parameterized form of the mean ROE used in this paper is given as[23]

$$\boldsymbol{x}_{\text{ROE}}=a_c\begin{bmatrix}\delta a\\ \delta\lambda\\ \delta e_x\\ \delta e_y\\ \delta i_x\\ \delta i_y\end{bmatrix}=a_c\begin{bmatrix}\dfrac{a_t-a_c}{a_c}\\ u_t-u_c+(\Omega_t-\Omega_c)\cos i_c\\ e_t\cos\omega_t-e_c\cos\omega_c\\ e_t\sin\omega_t-e_c\sin\omega_c\\ i_t-i_c\\ (\Omega_t-\Omega_c)\sin i_c\end{bmatrix} \tag{9}$$

where a, e, i, Ω, ω, and M are the classic Kepler orbital elements; δa represents the relative semi-major axis, $\delta\lambda$ the relative mean longitude, $u=M+\omega$ the mean argument of latitude, $\delta\boldsymbol{e}=(\delta e_x,\ \delta e_y)^{\mathrm{T}}$ the relative eccentricity vector, and $\delta\boldsymbol{i}=(\delta i_x,\ \delta i_y)^{\mathrm{T}}$ the relative inclination vector.

The set of ROE is particularly suitable for the problems of angles-only navigation because the weakly observable inter-satellite distance is almost

equal to the component $a\delta\lambda$. The relative dynamics model established based on ROE is effective for circular orbits (i.e., $e_c = 0$), but it is still singular for equatorial orbits (i.e., $i_c = 0$)[24]. For orbits with arbitrary eccentricity, the STM defined by the mean ROE including J_2 perturbations, the atmospheric drag, and the solar radiation pressure, and the third body gravity is obtained. In the case of only J_2 perturbations, the STM over the time interval $[t_0, t_f]$ is expressed as[25]

$$\boldsymbol{\Phi}(t_f,t_0)=\begin{bmatrix} 1 & 0 & 0 & 0 & 0 & 0 \\ -\frac{7}{2}\kappa EP\tau-\frac{3}{2}n\tau & 1 & \kappa e_{x0}FGP\tau & \kappa e_{y0}FGP\tau & -\kappa FS\tau & 0 \\ \frac{7}{2}\kappa e_{yf}Q\tau & 0 & \cos(\bar{\omega}\tau)-4\kappa e_{x0}e_{yf}GQ\tau & -\sin(\bar{\omega}\tau)-4\kappa e_{y0}e_{yf}GQ\tau & 5\kappa e_{yf}S\tau & 0 \\ -\frac{7}{2}\kappa e_{xf}Q\tau & 0 & \sin(\bar{\omega}\tau)+4\kappa e_{x0}e_{xf}GQ\tau & \cos(\bar{\omega}\tau)+4\kappa e_{y0}e_{xf}GQ\tau & -5\kappa e_{xf}S\tau & 0 \\ 0 & 0 & 0 & 0 & 1 & 0 \\ \frac{7}{2}\kappa S\tau & 0 & -4\kappa e_{x0}GS\tau & -4\kappa e_{y0}GS\tau & 2\kappa T\tau & 1 \end{bmatrix} \tag{10}$$

where $\kappa=\frac{\gamma}{a^{7/2}\eta^4}$, $\eta=\sqrt{1-\|\boldsymbol{e}\|^2}$, $\kappa=\frac{\gamma}{a^{7/2}\eta^4}$, $\eta=\sqrt{1-\|\boldsymbol{e}\|^2}$, $\gamma=\frac{3}{4}J_2R_e^2\sqrt{\mu}$, $G=\frac{1}{\eta^2}$, $F=4+3\eta$, $E=1+\eta$, $Q=5\cos^2 i-1$, $\bar{\omega}=\kappa Q$, $T=\sin^2 i$, $P=3\cos^2 i-1$, $S=\sin 2i$. The subscripts 0 and f represent the initial and the final values of the orbital elements of the chaser spacecraft, respectively; e_x and e_y the x and the y components of the absolute eccentricity vector $\boldsymbol{e}$. μ is the Earth's gravitational constant and R_e the Earth's equator radius.

For a near-circular orbit (i.e., $e_c \approx 0$), the STM given by Eq.(7) can be simplified as[26]

$$\boldsymbol{\Phi}(t_f,t_0)=\begin{bmatrix} 1 & 0 & 0 & 0 & 0 & 0 \\ -\frac{7\kappa EP+3n}{2}\tau & 1 & 0 & 0 & -\kappa FS\tau & 0 \\ 0 & 0 & \cos(\bar{\omega}\tau) & -\sin(\bar{\omega}\tau) & 0 & 0 \\ 0 & 0 & \sin(\bar{\omega}\tau) & \cos(\bar{\omega}\tau) & 0 & 0 \\ 0 & 0 & 0 & 0 & 1 & 0 \\ \frac{7}{2}\kappa S\tau & 0 & 0 & 0 & 2\kappa T\tau & 1 \end{bmatrix} \tag{11}$$

The argument of latitude u of the chaser spacecraft could also be used as the independent variable instead of time, and the τ in Eq.(11) can also be expressed as[24]

$$\tau=\frac{\Delta u}{n+\kappa(\eta P+Q)} \tag{12}$$

where Δu is the change in the argument of the latitude of the chaser spacecraft over the time interval $[t_0, t_f]$.

2 LoS Measurement Equations

The LoS vectors of the space target relative to the chaser spacecraft are modeled as a function of state variables, and the general form of the non-linear measurement model $\boldsymbol{h}$ is recorded as

$$\boldsymbol{z}(t)=\boldsymbol{h}(\boldsymbol{x}(t),t) \tag{13}$$

where the non-linear measurement model $\boldsymbol{h}$ depends on the state variable $\boldsymbol{x}$.

2.1 Rectilinear state LoS measurement equation

Before defining the LoS measurement vectors, the camera frame "cam" needs to be defined. Without loss of generality, it is assumed that the camera fixed boresight is aligned with the anti-flight direction. Under this assumption, the relationship between the relative position vectors in the camera frame "cam" and the Cartesian frame "car" are given as

$$\boldsymbol{r}_{\text{cam}}=\begin{bmatrix} 1 & 0 & 0 \\ 0 & 0 & 1 \\ 0 & -1 & 0 \end{bmatrix}\boldsymbol{r}_{\text{rec}}=\boldsymbol{R}_{\text{car}}^{\text{cam}}\boldsymbol{r}_{\text{rec}} \tag{14}$$

The LoS vector could be represented by a set

of azimuth α and elevation ε, which can be expressed as a function of the relative position vector $\boldsymbol{r}_{\text{cam}}$ in the camera frame, as shown in Fig.2. Thus, the rectilinear state LoS measurement equation can be expressed as

$$\boldsymbol{h}(\boldsymbol{x}_{\text{rec}})=\begin{pmatrix}\alpha\\ \varepsilon\end{pmatrix}=\begin{pmatrix}\arcsin\left(r_y^{\text{cam}}/\|\boldsymbol{r}^{\text{cam}}\|\right)\\ \arctan\left(r_x^{\text{cam}}/r_z^{\text{cam}}\right)\end{pmatrix} \tag{15}$$

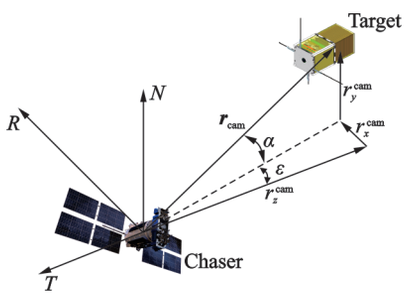

Fig.2 LoS measurement geometry

2.2 Curvilinear state LoS measurement equation

The LoS vector defined by the curvilinear state $\boldsymbol{x}_{\text{cur}}$ is calculated through mapping the curvilinear state $\boldsymbol{x}_{\text{cur}}$ to the rectilinear state $\boldsymbol{x}_{\text{rec}}$ and applying Eqs. (14—15). The mapping relationship between the rectilinear state and the curvilinear state is given as

$$\begin{cases}x=(a+r)\cos\psi\cos\theta-a\\ y=(a+r)\cos\psi\sin\theta\\ z=(a+r)\sin\psi\end{cases} \tag{16}$$

2.3 ROE state LoS measurement equation

In order to define the LoS vector by the ROE state, it is necessary to map the ROE state to the rectilinear state. Four different mapping relationships are considered in this paper: (1) The ROE state is linearly mapped to the rectilinear state, which is recorded as the measurement model h_1; (2) the ROE state is linearly mapped to the curvilinear state, and then the curvilinear state is mapped to the rectilinear state, which is recorded as the measurement model h_2; (3) the ROE state is non-linearly mapped to the rectilinear state, which is recorded as the measurement model h_3; (4) the ROE state is non-linearly mapped to the rectilinear state with the transformation from the mean orbital elements to the osculating orbital elements[27], which is recorded as the measurement model h_4. For the measurement model h_3, the ROE state and the absolute orbital elements of the chaser spacecraft are used to calculate the absolute orbital elements of the space target. Then, the absolute position vectors of the chaser spacecraft and the space target are calculated in the geocentric inertial frame according to their absolute orbital elements. Finally, the relative position vectors in the Cartesian frame are obtained according to the absolute position vectors of the chaser spacecraft and the space target in the geocentric inertial frame. The linear map between the ROE state and the rectilinear or curvilinear state is formulated by treating the ROE as the integration constant of the HCW equation[28]. If necessary, Eq. (16) can be used to map the curvilinear state to the relative position vector in the Cartesian frame. The mapping relationship between the ROE state and the translational state is given as

$$\boldsymbol{x}_{\text{cur/rec}}=\boldsymbol{\Pi}(t)\boldsymbol{x}_{\text{ROE}}=\begin{bmatrix}1&0&-\cos u_c&-\sin u_c&0&0\\ 0&1&2\sin u_c&-2\cos u_c&0&0\\ 0&0&0&0&\sin u_c&-\cos u_c\\ 0&0&n\sin u_c&-n\cos u_c&0&0\\ -1.5n&0&2n\cos u_c&2n\sin u_c&0&0\\ 0&0&0&0&n\cos u_c&n\sin u_c\end{bmatrix}\boldsymbol{x}_{\text{ROE}} \tag{17}$$

3 Observability Analysis of Angles-Only Navigation Based on Gramian Matrix

An observability analysis theory based on the Gramian matrix is introduced to determine which relative dynamics model could maximize the observability of angles-only navigation. Assume that the relative motion state at time t_0 is $\boldsymbol{x}(t_0)$, and k LoS measurements are performed between the time t_1 and t_k, we can obtain the measurement vector $\boldsymbol{Z}$ as

$$Z=\begin{pmatrix} z(t_1) \\ z(t_2) \\ \vdots \\ z(t_k) \end{pmatrix}=\begin{pmatrix} \boldsymbol{h}(\boldsymbol{\Phi}(t_1,t_0)\boldsymbol{x}(t_0),t_1) \\ \boldsymbol{h}(\boldsymbol{\Phi}(t_2,t_0)\boldsymbol{x}(t_0),t_2) \\ \vdots \\ \boldsymbol{h}(\boldsymbol{\Phi}(t_k,t_0)\boldsymbol{x}(t_0),t_k) \end{pmatrix} \tag{18}$$

In order to prove that the angles-only navigation system has local weak observability, it can be proved that the partial derivative matrix χ of the LoS measurements relative to the disturbance state at the reference time is full rank, and χ can be expressed as

$$\chi=\frac{\partial Z}{\partial \boldsymbol{x}}\bigg|_{\boldsymbol{x}(t_0)}=\begin{pmatrix} \dfrac{\partial \boldsymbol{h}}{\partial \boldsymbol{x}}(\boldsymbol{\Phi}(t_1,t_0)\boldsymbol{x}(t_0),t_1) \\ \dfrac{\partial \boldsymbol{h}}{\partial \boldsymbol{x}}(\boldsymbol{\Phi}(t_2,t_0)\boldsymbol{x}(t_0),t_2) \\ \vdots \\ \dfrac{\partial \boldsymbol{h}}{\partial \boldsymbol{x}}(\boldsymbol{\Phi}(t_k,t_0)\boldsymbol{x}(t_0),t_k) \end{pmatrix}=$$

$$\begin{pmatrix} H(\boldsymbol{\Phi}(t_1,t_0)\boldsymbol{x}(t_0),t_1)\boldsymbol{\Phi}(t_1,t_0) \\ H(\boldsymbol{\Phi}(t_2,t_0)\boldsymbol{x}(t_0),t_2)\boldsymbol{\Phi}(t_2,t_0) \\ \vdots \\ H(\boldsymbol{\Phi}(t_k,t_0)\boldsymbol{x}(t_0),t_k)\boldsymbol{\Phi}(t_k,t_0) \end{pmatrix} \tag{19}$$

where

$$H(\boldsymbol{x}(t),t)=\frac{\partial \boldsymbol{h}}{\partial \boldsymbol{x}}\bigg|_{\boldsymbol{x}(t)} \tag{20}$$

In addition, the observability of angles-only navigation can also be judged according to the condition number of the Gramian matrix, which is expressed as cond$(\chi^{\mathrm{T}}\chi)$. The larger the cond$(\chi^{\mathrm{T}}\chi)$, the worse the observability of angles-only navigation.

3.1 Rectilinear state measurement sensitivity matrix $\boldsymbol{H}_{\mathrm{rec}}$

In order to calculate the measurement sensitivity matrix $\boldsymbol{H}_{\mathrm{rec}}$ of the LoS measurements relative to the rectilinear state, the measurement sensitivity matrix of the LoS measurements relative to the relative position vector in the camera frame needs to be calculated. According to the Ref.[29], it is given as

$$\frac{\partial \boldsymbol{h}}{\partial \boldsymbol{r}_{\mathrm{cam}}}\bigg|_{\boldsymbol{r}_{\mathrm{cam}}(t)}=\frac{1}{\|\boldsymbol{r}_{\mathrm{cam}}\|}\begin{bmatrix} -\sin\varepsilon\sin\alpha & \cos\varepsilon & -\sin\varepsilon\cos\alpha \\ \dfrac{\cos\alpha}{\cos\varepsilon} & 0 & -\dfrac{\sin\alpha}{\cos\varepsilon} \end{bmatrix} \tag{21}$$

Using Eq.(14) to map the partial derivative obtained from Eq.(21) to the Cartesian frame, we obtain the rectilinear state measurement sensitivity matrix $\boldsymbol{H}_{\mathrm{rec}}$ as

$$\boldsymbol{H}_{\mathrm{rec}}(\boldsymbol{x}_{\mathrm{rec}})=\frac{\partial \boldsymbol{h}}{\partial \boldsymbol{r}_{\mathrm{cam}}}\bigg|_{\boldsymbol{r}_{\mathrm{cam}}}\cdot\boldsymbol{R}_{\mathrm{car}}^{\mathrm{cam}}=$$

$$\frac{1}{\|\boldsymbol{r}_{\mathrm{cam}}\|}\begin{bmatrix} -\sin\varepsilon\sin\alpha & \sin\varepsilon\cos\alpha & \cos\varepsilon \\ \dfrac{\cos\alpha}{\cos\varepsilon} & \dfrac{\sin\alpha}{\cos\varepsilon} & 0 \end{bmatrix} \tag{22}$$

3.2 Curvilinear state measurement sensitivity matrix $\boldsymbol{H}_{\mathrm{cur}}$

The curvilinear state measurement sensitivity matrix $\boldsymbol{H}_{\mathrm{cur}}$ is the product of the rectilinear state measurement sensitivity matrix $\boldsymbol{H}_{\mathrm{rec}}$ evaluated at the relative position vector computed using Eq.(16) and the partial derivative of the rectilinear state with respect to the current curvilinear state, namely

$$\boldsymbol{H}_{\mathrm{cur}}(\boldsymbol{x}_{\mathrm{cur}})=\boldsymbol{H}_{\mathrm{rec}}(\boldsymbol{x}_{\mathrm{rec}})\frac{\partial \boldsymbol{x}_{\mathrm{rec}}}{\partial \boldsymbol{x}_{\mathrm{cur}}}\bigg|_{\boldsymbol{x}_{\mathrm{cur}}(t)} \tag{23}$$

where

$$\frac{\partial \boldsymbol{x}_{\mathrm{rec}}}{\partial \boldsymbol{x}_{\mathrm{cur}}}\bigg|_{\boldsymbol{x}_{\mathrm{cur}}(t)}=\begin{bmatrix} \cos\psi\cos\theta & -\left(\dfrac{r}{a}+1\right)\cos\psi\sin\theta & -\left(\dfrac{r}{a}+1\right)\sin\psi\cos\theta \\ \cos\psi\sin\theta & \left(\dfrac{r}{a}+1\right)\cos\psi\cos\theta & -\left(\dfrac{r}{a}+1\right)\sin\psi\sin\theta \\ \sin\psi & 0 & \left(\dfrac{r}{a}+1\right)\cos\psi \end{bmatrix} \tag{24}$$

3.3 ROE state measurement sensitivity matrix $\boldsymbol{H}_{\mathrm{ROE}}$

For the case of linearly mapping the ROE state to the rectilinear state, the measurement sensitivity matrix $\boldsymbol{H}_{\mathrm{ROE}}^{\mathrm{rec}}$ is the product of the rectilinear state measurement sensitivity matrix $\boldsymbol{H}_{\mathrm{rec}}$ evaluated at $\boldsymbol{\Pi}(t)\boldsymbol{x}_{\mathrm{ROE}}$ and the partial derivative of the rectilinear state with respect to the ROE state, namely

$$\boldsymbol{H}_{\mathrm{ROE}}^{\mathrm{rec}}(\boldsymbol{x}_{\mathrm{ROE}})=\boldsymbol{H}_{\mathrm{rec}}(\boldsymbol{\Pi}(t)\boldsymbol{x}_{\mathrm{ROE}})\frac{\partial \boldsymbol{x}_{\mathrm{rec}}}{\partial \boldsymbol{x}_{\mathrm{ROE}}}\bigg|_{\boldsymbol{x}_{\mathrm{ROE}}(t)} \tag{25}$$

For the case of linearly mapping the ROE state to the curvilinear state, the curvilinear state is then mapped to the rectilinear state. The measurement sensitivity matrix $\boldsymbol{H}_{\mathrm{ROE}}^{\mathrm{cur}}$ is the product of the curvilinear state measurement sensitivity matrix $\boldsymbol{H}_{\mathrm{cur}}$ evaluated at $\boldsymbol{\Pi}(t)\boldsymbol{x}_{\mathrm{ROE}}$ and the partial derivative of the curvilinear state with respect to the ROE state, namely

$$\boldsymbol{H}_{\mathrm{ROE}}^{\mathrm{cur}}(\boldsymbol{x}_{\mathrm{ROE}})=\boldsymbol{H}_{\mathrm{cur}}(\boldsymbol{\Pi}(t)\boldsymbol{x}_{\mathrm{ROE}})\frac{\partial \boldsymbol{x}_{\mathrm{cur}}}{\partial \boldsymbol{x}_{\mathrm{ROE}}}\bigg|_{\boldsymbol{x}_{\mathrm{ROE}}(t)} \tag{26}$$

For the case of non-linearly mapping the ROE state to the rectilinear state, the absolute orbital elements of the space target is calculated by the ROE state and the absolute orbital elements of the chaser spacecraft to obtain the relative position vector in the Cartesian frame, and the nonlinear mapping relationship is denoted as $\boldsymbol{g}(\boldsymbol{x}_{\mathrm{ROE}}(t),\boldsymbol{e}_{co}(t))$. The measurement sensitivity matrix $\boldsymbol{H}_{\mathrm{ROE}}^{\mathrm{non}}$ is the product of the rectilinear measurement sensitivity matrix $\boldsymbol{H}_{\mathrm{rec}}$ evaluated at $\boldsymbol{g}(\boldsymbol{x}_{\mathrm{ROE}}(t),\boldsymbol{e}_{co}(t))$ and the partial derivative of the rectilinear state with respect to the ROE state, namely

$$\boldsymbol{H}_{\mathrm{ROE}}^{\mathrm{non}}(\boldsymbol{x}_{\mathrm{ROE}})=\boldsymbol{H}_{\mathrm{rec}}\big(\boldsymbol{g}(\boldsymbol{x}_{\mathrm{ROE}}(t),\boldsymbol{e}_{co}(t))\big)\frac{\partial \boldsymbol{x}_{\mathrm{rec}}}{\partial \boldsymbol{x}_{\mathrm{ROE}}}\bigg|_{\boldsymbol{x}_{\mathrm{ROE}}(t)} \tag{27}$$

Finally, the measurement sensitivity matrix in Eqs.(25—27) could be approximated as follows

$$\frac{\partial \boldsymbol{x}_{\mathrm{rec/cur}}}{\partial \boldsymbol{x}_{\mathrm{ROE}}}\bigg|_{\boldsymbol{x}_{\mathrm{ROE}}(t)}=\boldsymbol{\Pi}(t) \tag{28}$$

4 Adaptive Extended Kalman Filter

Extended Kalman filter (EKF)[30] is used to perform real-time filtering of the relative motion states between the chaser spacecraft and the space target. EKF uses a linear approach to transform a nonlinear system into an approximate linear system. The statistics of the process and measurement noises are critical to the stability and performances of the EKF. Thus, proper selection of the statistics of the process and measurement noises can improve the accuracy of dynamic relative state estimation.

This paper introduces the "innovation" covariance matching method[31] to adjust the measurement noises online to solve the problem that the angles-only navigation filter using non-linear dynamics method is sensitive to the measurement noises. The basic idea of the "innovation" covariance matching method is to use the statistical and theoretical values of the sample to infer the measurement noises of the Kalman filter and make adaptive adjustments. The measurement prediction error of the Kalman filter is also called "innovation" or "residual"[32] can be given by

$$\boldsymbol{\Delta}_k=\boldsymbol{z}_k-\boldsymbol{h}(\hat{\boldsymbol{x}}_{k|(k-1)})\approx\boldsymbol{z}_k-\boldsymbol{H}_k\hat{\boldsymbol{x}}_{k|(k-1)} \tag{29}$$

where $\hat{\boldsymbol{x}}_{k|(k-1)}$ denotes the priori state estimation; $\boldsymbol{H}_k$ the measurement sensitivity matrix; and $\boldsymbol{z}_k$ the measurement model and can be given by

$$\boldsymbol{z}_k=\boldsymbol{H}_k\boldsymbol{x}_{k|k}+\boldsymbol{v}_k \tag{30}$$

where $\hat{\boldsymbol{x}}_{k|k}$ denotes the posterior state estimation; $\boldsymbol{v}_k$ a zero mean white noise that denotes the measurement noise of the navigation system.

By substituting Eq.(30) into Eq.(29), one can obtain "innovation" as

$$\boldsymbol{\Delta}_k\approx\boldsymbol{H}_k\big(\boldsymbol{x}_{k|k}-\hat{\boldsymbol{x}}_{k|(k-1)}\big)+\boldsymbol{v}_k \tag{31}$$

The theoretical covariance $\boldsymbol{\Sigma}_{\boldsymbol{\Delta}_k}$of $\boldsymbol{\Delta}_k$can be obtained by applying the following expectation operator

$$\boldsymbol{\Sigma}_{\boldsymbol{\Delta}_k}=E[\boldsymbol{\Delta}_k\boldsymbol{\Delta}_k^{\mathrm{T}}]=\boldsymbol{H}_k\hat{\boldsymbol{P}}_{k|(k-1)}\boldsymbol{H}_k^{\mathrm{T}}+\boldsymbol{R}_k \tag{32}$$

where $\boldsymbol{R}_k$ denotes the measurement noise covariance matrix; $\hat{\boldsymbol{P}}_{k|(k-1)}$ the covariance corresponding to $\hat{\boldsymbol{x}}_{k|(k-1)}$.

On the other hand, if a sample of N innovations is collected in a sliding window, the sample covariance $\hat{\boldsymbol{\Sigma}}_{\boldsymbol{\Delta}_k}$ of the sample can be calculated as

$$\hat{\boldsymbol{\Sigma}}_{\boldsymbol{\Delta}_k}=\frac{1}{N}\sum_{i=k-N+1}^{k}\boldsymbol{\Delta}_i\boldsymbol{\Delta}_i^{\mathrm{T}} \tag{33}$$

According to the equivalent relationship of Eq.(32) and Eq.(33), the estimation of the measurement noise covariance matrix $\hat{\boldsymbol{R}}_k$ is calculated as

$$\hat{\boldsymbol{R}}_k=\frac{1}{N}\sum_{i=k-N+1}^{k}\boldsymbol{\Delta}_i\boldsymbol{\Delta}_i^{\mathrm{T}}-\boldsymbol{H}_k\hat{\boldsymbol{P}}_{k|(k-1)}\boldsymbol{H}_k^{\mathrm{T}} \tag{34}$$

Then

$$\Delta\boldsymbol{R}_k=\hat{\boldsymbol{R}}_k-\boldsymbol{R}_k=\frac{1}{N}\sum_{i=k-N+1}^{k}\boldsymbol{\Delta}_i\boldsymbol{\Delta}_i^{\mathrm{T}}-\boldsymbol{H}_k\hat{\boldsymbol{P}}_{k|(k-1)}\boldsymbol{H}_k^{\mathrm{T}}-\boldsymbol{R}_k \tag{35}$$

Finally, the corrected measurement noise covariance matrix is obtained as

$$\tilde{R}_k = R_k + \Delta R_k \tag{36}$$

5 Numerical Simulation

5.1 Problem configuration

The theoretical relative motion states between the chaser spacecraft and the space target are numerically propagated using a 20 × 20 gravity field and including J_2 perturbations, the solar radiation pressure, the third-body and atmospheric drag perturbations. A set of LoS measurements is finally created from the theoretical relative motion states. In this paper, the performances of the proposed angles-only navigation architecture are tested by means of numerical simulations. The numerical simulation is mainly carried out in three typical orbital scenarios: ROE1 which represents a possible configuration for the beginning of an approach to an non-cooperative space target, ROE2 which presents a drift of almost 1 km per orbit toward an non-cooperative space target; ROE3 which represents the starting point of a docking phase. The main simulation parameters are shown in Table 1. The relative motion trajectories are shown in Fig.3.

Table 1 Main simulation parameters

Parameter	Value
Absolute orbital elements of the space target (a, e, i, Ω, ω, M)	(6878.137 km, 0, 40°, 120°, 0°, 50°)
Initial relative orbital elements ROE1 ($a\delta a$, $a\delta\lambda$, $a\delta e_x$, $a\delta e_y$, $a\delta i_x$, $a\delta i_y$)/km	(0, −30, 0.5, 0, −0.5, 0)
Initial relative orbital elements ROE2 ($a\delta a$, $a\delta\lambda$, $a\delta e_x$, $a\delta e_y$, $a\delta i_x$, $a\delta i_y$)/km	(−0.15, −20, 0.3, 0, −0.3, 0)
Initial relative orbital elements ROE3 ($a\delta a$, $a\delta\lambda$, $a\delta e_x$, $a\delta e_y$, $a\delta i_x$, $a\delta i_y$)/km	(0, −5, 0, 0, 0, 0)
Total filtering time t_f/s	3 000
Standard deviation of LoS measurement ($\sigma_\alpha = \sigma_\varepsilon$)/arc sec	18
Standard deviation of satellite attitude measurement ($\sigma_{\text{att, off-axis}}$, $\sigma_{\text{att, roll}}$)/arc sec	(6, 40)
GPS position measurement error/km	0.01
GPS velocity measurement error/(km·s^{-1})	1×10^{-4}

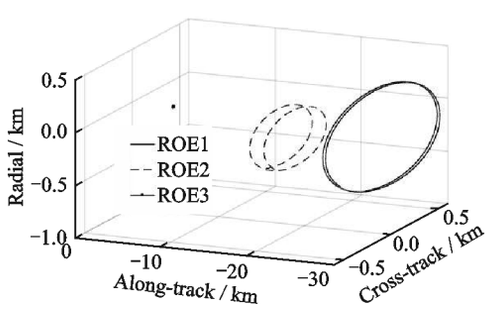

Fig.3 Relative trajectories in three typical orbital scenarios

5.2 Simulation results and analysis

5.2.1 Simulation results of the observability analysis of angles-only navigation

This study compares and analyzes the observability of angles-only navigation under three relative dynamics models, including the rank of the matrix χ and the condition number cond($\chi^T\chi$) of the Gramian matrix. In the process of analyzing the observability of angles-only navigation, the variables include not only various relative dynamics and measurement models, but also the sampling period and total sampling time. First, a comparative analysis of the observability of angles-only navigation under the rectilinear and curvilinear state relative dynamics models is carried out, and the results are shown in Tables 2—4. Table 2 shows the results of the observability analysis of angles-only navigation when the sampling period is 10 s and the total sampling time is 1 000 s under the rectilinear and curvilinear state relative dynamics models, including the rank of the matrix χ and the condition number cond($\chi^T\chi$) of the

Table 2 Observability analysis of angles-only navigation when the sampling period is 10 s and the total sampling time is 1 000 s under the rectilinear and curvilinear state relative dynamics models

Scenario	rank(χ)		cond($\chi^T\chi$)	
	Rectilinear	Curvilinear	Rectilinear	Curvilinear
ROE1	5	6	2.07×10^{18}	8.00×10^{17}
ROE2	5	6	1.05×10^{18}	6.55×10^{17}
ROE3	5	6	4.36×10^{18}	1.38×10^{18}

Gramian matrix; Table 3 shows the condition number cond($\chi^{\mathrm{T}}\chi$) of the Gramian matrix under the rectilinear and curvilinear state relative dynamics models, the total sampling time is 1 000 s, and the different sampling periods; Table 4 shows the condition number cond($\chi^{\mathrm{T}}\chi$) of the Gramian matrix under the rectilinear and curvilinear state relative dynamics models, the sampling period is 10 s, and the different total sampling time.

Table 3 Condition number cond($\chi^{\mathrm{T}}\chi$) of the Gramian matrix under the rectilinear and curvilinear state relative dynamics models with the total sampling time of 1 000 s and different sampling periods

Scenario	10 s		50 s		100 s	
	Rectilinear	Curvilinear	Rectilinear	Curvilinear	Rectilinear	Curvilinear
ROE1	2.07×10^{18}	8.00×10^{17}	2.20×10^{18}	2.51×10^{17}	1.83×10^{18}	1.97×10^{17}
ROE2	1.05×10^{18}	6.55×10^{17}	1.14×10^{18}	1.54×10^{17}	5.27×10^{17}	1.17×10^{17}
ROE3	4.36×10^{18}	1.38×10^{18}	8.49×10^{18}	2.12×10^{18}	1.21×10^{19}	2.74×10^{18}

Table 4 Condition number cond($\chi^{\mathrm{T}}\chi$) of the Gramian matrix under the rectilinear and curvilinear state relative dynamics models with the sampling period of 10 s and different total sampling time

Scenario	100 s		500 s		1 000 s	
	Rectilinear	Curvilinear	Rectilinear	Curvilinear	Rectilinear	Curvilinear
ROE1	2.06×10^{19}	6.65×10^{18}	5.05×10^{18}	2.34×10^{18}	2.07×10^{18}	8.00×10^{17}
ROE2	1.44×10^{19}	6.09×10^{18}	4.04×10^{18}	1.18×10^{18}	1.05×10^{18}	6.55×10^{17}
ROE3	2.71×10^{20}	8.70×10^{18}	8.86×10^{18}	4.71×10^{18}	4.36×10^{18}	1.38×10^{18}

It can be seen from Table 2 that the matrix χ under the rectilinear state relative dynamics model is not full rank, so the rectilinear state relative dynamics model cannot provide complete observability for angles-only navigation. In addition, comparing and analyzing the condition number cond ($\chi^{\mathrm{T}}\chi$) of the Gramian matrix, it can be concluded that the observability of angles-only navigation in ROE1 and ROE2 is better than that in ROE3. In addition, matrix χ under the curvilinear state relative dynamics model is full rank, so the curvilinear state relative dynamics model can provide complete observability for the angles-only navigation system. It can be seen from Table 3 that when other conditions are fixed, the sampling period has a relatively small effect on the observability of angles-only navigation, and the maximum and minimum condition number of the Gramian matrix do not exceed one order of magnitude, which indicates that the performances of the angles-only navigation system are robust against low sampling rates or short-term data interruptions. It can be seen from Table 4 that when other conditions are fixed, the greater the total sampling time, the better the observability of the angles-only navigation system. Thus, the observability of angles-only navigation can be improved by increasing the total sampling time.

In addition, the observabilities of angles-only navigation under the ROE state relative dynamics model with four measurement models are compared and analyzed, and the results are shown in Tables 5—6. Table 5 shows that in the results of the observability analysis of angles-only navigation under the simplified and complex STM with the measurement model h_1, the sampling period is 10 s, and the total sampling time is 1 000 s; Table 6 shows the results of the observability analysis of angles-only navigation under the simplified STM with four measurement models. The sampling period is 10 s, and the total sampling time is 1 000 s.

It can be seen from Table 5 that the matrix χ under the measurement model h_1 is not full rank, so the angles-only measurement navigation system is not completely observable. In addition, the difference between the condition number of the Gramian matrix under the complex and simplified STM is very small. Thus, in order to save the resources of on-board computer, it is completely reasonable to use a simplified STM for near-circular orbits. It can be seen from Table 6 that the measurement models

Table 5 Observability analysis of angles-only navigation under the simplified and complex STM with the measurement model h_1 when the sampling period is 10 s, and the total sampling time is 1 000 s

Scenario	rank(χ)		cond($\chi^T\chi$)	
	Simplified STM	Complex STM	Simplified STM	Complex STM
ROE1	5	5	1.76×10^{18}	1.75×10^{18}
ROE2	5	5	5.83×10^{17}	5.82×10^{17}
ROE3	5	5	6.08×10^{18}	6.08×10^{18}

Table 6 Observability analysis of angles-only navigation under the simplified STM with four measurement models when the sampling period is 10 s and the total sampling time is 1 000 s

Scenario	rank(χ)				cond($\chi^T\chi$)			
	h_1	h_2	h_3	h_4	h_1	h_2	h_3	h_4
ROE1	5	6	6	6	1.76×10^{18}	4.85×10^{12}	4.47×10^{12}	3.82×10^{11}
ROE2	5	6	6	6	5.83×10^{17}	2.16×10^{12}	2.07×10^{12}	1.75×10^{11}
ROE3	5	6	6	6	6.08×10^{18}	7.94×10^{13}	7.33×10^{13}	5.69×10^{12}

h_2, h_3, and h_4 can provide complete observability for the angles-only navigation system, and the condition number of the Gramian matrix under the measurement model h_4 is smaller than those of the other three scenarios. Thus, the transformation from the mean orbital elements to the osculating orbital elements can also improve the observability of angles-only navigation.

5.2.2 Simulation results of the angles-only navigation filter

This paper also compares and analyzes the performances of the angles-only navigation filter under different relative dynamics and measurement models in ROE1, and the results are shown in Figs. 4—7. Fig. 4 shows the estimation errors of the angles-only navigation filter under the rectilinear state relative dynamics model. Fig. 5 shows the estimation errors of the angles-only navigation filter under the curvilinear state relative dynamics model. The estimation errors of the angles-only navigation filter under the ROE state relative dynamics model with four measurement models are compared and analyzed, and the results are shown in Fig. 6. In addition, the estimation errors of the angles-only navigation filter under the rectilinear state relative dynamics model and the ROE state relative dynamics model with the measurement model h_4 are compared and analyzed, and the results are shown in Fig. 7.

It can be seen from Fig. 4 that the angles-only navigation filter under the rectilinear state relative dynamics model cannot converge to the true inter-satellite range, and it exhibits continuous oscillation errors during the entire simulation process. It can be seen from Fig. 5 that the angles-only navigation filter under the curvilinear state relative dynamics model can slowly converge to the true inter-satellite range, and the errors of the other state elements show the same oscillation as the orbital period. In addition, the oscillation amplitude of the errors of the relative velocity in tangential direction is twice the oscillation amplitude of the errors of the relative velocity in radial direction, and they are out of phase with each other. Thus, the above results show that the geometric shape of the relative motion are observable.

It can be seen from Fig. 6 that under the ROE state relative dynamics model, the estimation errors of the angles-only navigation filter with the measurement model h_1 cannot converge to the true $a\delta\lambda$, while the angles-only navigation filter with the measurement models h_2, h_3, and h_4 can converge to the true $a\delta\lambda$, and the angles-only navigation filter with the measurement models h_3 and h_4 can reduce the estimation errors of $a\delta\lambda$ to a few hundred meters. In addition, it can be seen from Fig. 6 that the transformation from the mean orbital elements to the osculating orbital elements can also improve the performances of the angles-only navigation filter, which is also consistent with the conclusions drawn by the observability analysis theory of angles-only navigation based on the Gramian matrix. It can be seen

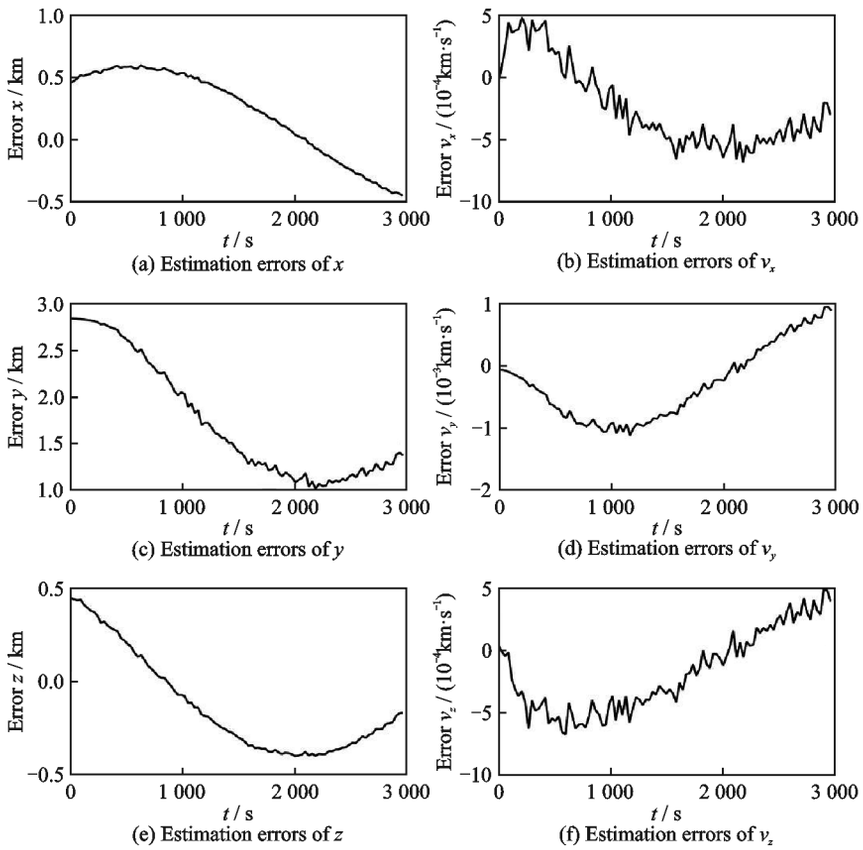

Fig.4 Estimation errors of the angles-only navigation filter under the rectilinear state relative dynamics model

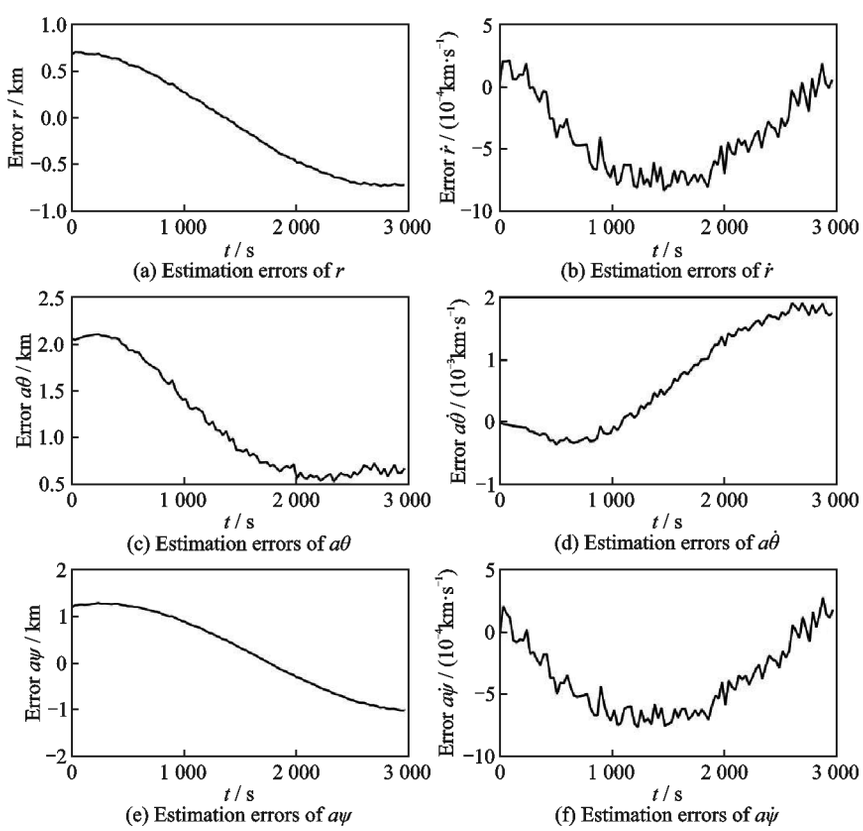

Fig.5 Estimation errors of the angles-only navigation filter under the curvilinear state relative dynamics model

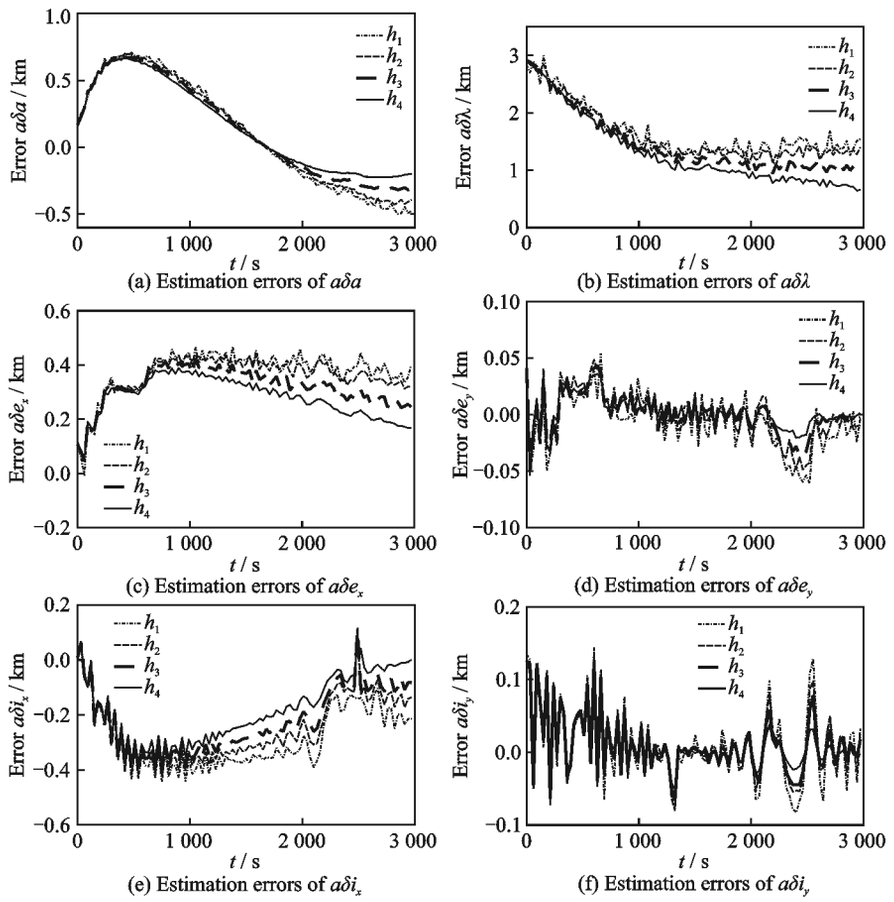

Fig.6 Estimation errors of the angles-only navigation filter under the ROE state relative dynamics model with four measurement models

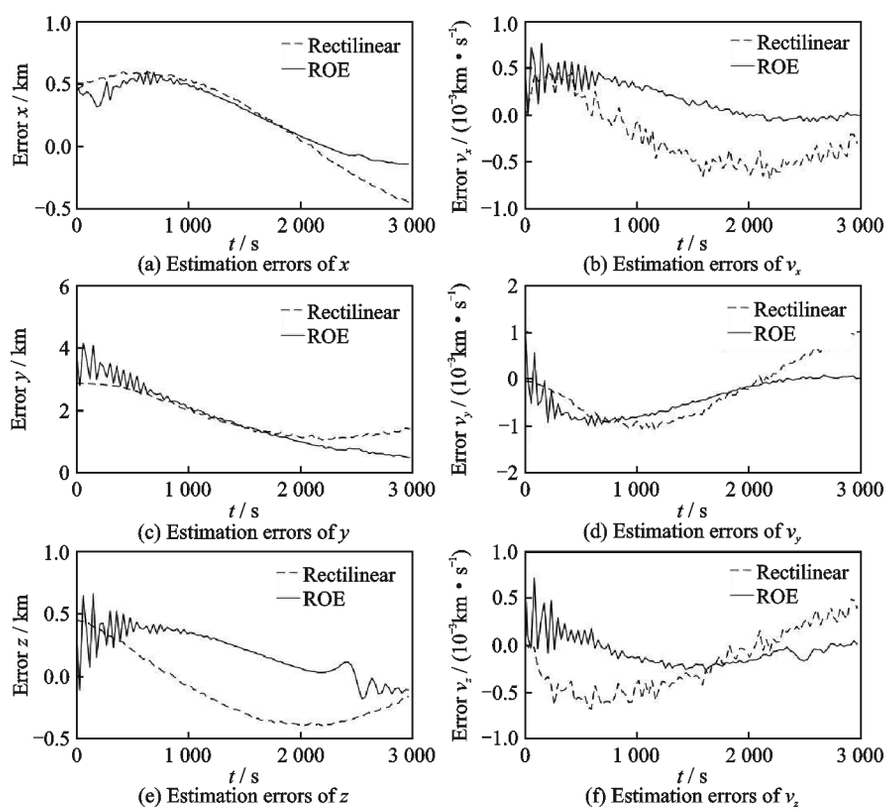

Fig.7 Estimation errors of the angles-only navigation filter under the rectilinear state relative dynamics model and the ROE state relative dynamics model with the measurement model h_4

from Fig.7 that the performances of the angles-only navigation filter under the ROE state relative dynamics model with the measurement model h_4 is significantly better than that under the rectilinear state relative dynamics model. The convergence rate is faster and the navigation accuracy is higher.

The above results further confirm the conclusions drawn by the observability analysis theory of angles-only navigation based on the Gramian matrix. That is, capturing the non-linearity of the system in the evolution of relative motion can improve the performances of the angles-only navigation filter. It demonstrates that the angles-only navigation filtering scheme without orbital or attitude maneuvering is completely feasible.

6 Conclusions

This paper proposes an angles-only navigation architecture using non-linear dynamics method for non-cooperative rendezvous of spacecraft. The angles-only navigation architecture improves the observability of angles-only navigation through capturing the non-linearity of the system in the evolution of relative motion. Then, the performances of the angles-only navigation architecture are tested in a high-fidelity simulation environment, and the following conclusions are drawn:

(1) The rectilinear state relative dynamics model cannot provide complete observability for angles-only navigation, while the curvilinear state relative dynamics model can. Thus, the curvilinear state relative dynamics model provides a novel scheme to solve the problem of poor observability of angles-only navigation.

(2) When other conditions are fixed, the sampling period has a relatively small effect on the observability of angles-only navigation. However, the condition number of the Gramian matrix can be reduced through increasing the total sampling time, so as to improve the observability of angles-only navigation.

(3) In the case of the ROE state relative dynamics model, including the non-linear mapping relationship from the ROE state to the rectilinear state and the transformation from the mean orbital elements to the osculating orbital elements in the LoS measurement equations can improve the observability of angles-only navigation.

Finally, the comparative analysis of the results of the performances of the angles-only navigation filter under different relative dynamics models further confirm the conclusions drawn through the observability analysis theory based on the Gramian matrix.

In a nutshell, this paper demonstrates that the angles-only navigation filtering scheme without orbital or attitude maneuvering is completely feasible through improving the modeling of the relative dynamics and LoS measurement equations. Thus, the angles-only navigation architecture using non-linear dynamics method proposed in this paper could provide theoretical guidelines for any missions that use angles-only navigation for non-cooperative rendezvous of spacecraft.

References

[1] RISTIC B, ARULAMPALAM M S. Tracking a manoeuvring target using angle-only measurements: Algorithms and performance[J]. Signal Processing, 2003, 83(6): 1223-1238.

[2] WAN W, WEI Y, GUO Z, et al. Toward a power of planetary science from a gaint of deep space exploration[J]. Bulletin of Chinese Academy of Science, 2019, 34(7): 748-755.

[3] ZHANG Y, WANG X, XI K, et al. Impact analysis of solar irradiance change on precision orbit determination of navigation satellites[J]. Transactions of Nanjing University of Aeronautics and Astronautics, 2019, 36(6): 889-901.

[4] WANG Y, WANG X, CUI N. Robust decentralised state estimation for formation flying spacecraft[J]. IET Radar, Sonar and Navigation, 2019, 13(5): 814-823.

[5] LIU R, LIU M, LIU Y. Nonlinear optimal tracking control of spacecraft formation flying with collision avoidance[J]. Transactions of the Institute of Measurement and Control, 2019, 41(4): 889-899.

[6] RAJA C. Autonomous orbital rendezvous using angles-only navigation[D]. Logan, USA: Utah State University, 2001.

[7] DEHANN F, BRENT E T, STEVE U, et al. Vi-

sion-based relative navigation and control for autonomous spacecraft inspection of an unknown object[C]// Proceedings of the Guidance, Navigation, and Control and Co-located Conferences. Boston, USA: AIAA, 2013.

[8] LIANG B, HE Y, ZHOU Y. Application of ToF camera in close-range measurement of uncooperative target in space[J]. Journal of Astronautics, 2016, 37(9): 1080-1088.

[9] GONG B, LI W, LI S, et al. Angles-only initial relative orbit determination algorithm for noncooperative spacecraft proximity operations[J]. Astrodynamics, 2018, 2(3): 217-231.

[10] GAIAS G, ARDAENS J S. Flight demonstration of autonomous noncooperative rendezvous in low earth orbit[J]. Journal of Guidance, Control, and Dynamics, 2018, 41(6): 1137-1354.

[11] WOFFINDEN D C, GELLER D K. Navigating the road to autonomous orbital rendezvous[J]. Journal of Spacecraft and Rockets, 2007, 44(4): 898-909.

[12] GE X, HUANG J, ZHOU Q, et al. Evaluation of space station on-orbit maintenance operation complexity and its experimental validation[J]. Journal of Beijing University of Aeronautics and Astronautics, 2019, 45(11): 2228-2236.

[13] DAVID V. Evaluating gooding angles-only orbit determination of space based space surveilliance measurements[C]//Proceedings of the 8th US/Russian Space Surveillance Workshop. [S.l.]:[s.n.], 2010.

[14] KEITH L. Space-based relative multitarget tracking[D]. Lola, USA: Missouri University of Science and Technology, 2015.

[15] ARDAENS J S, GAIAS G. A numerical approach to the problem of angles-only initial relative orbit determination in low earth orbit[J]. Advances in Space Research, 2019, 63: 3884-3899.

[16] WOFFINDEN D C. Angles-only navigation for autonomous orbital rendezvous[D]. Logan, USA: Utah State University, 2008.

[17] GONG B C. Research on angles-only relative orbit determination algorithms for spacecraft autonomous rendezvous[D]. Xi'an, China: Northwestern Polytechnical University, 2016.

[18] PI J, BANG H. Trajectory design for satellite relative angles-only navigation[C]//Proceedings of the 9th International Conference on Mathematical Problems in Engineering, Aerospace and Sciences. [S.l.]: [s.n.], 2012, 1493: 747-751.

[19] JAGAT A, SINCLAIR A. Control of spacecraft relative motion using angles-only navigation[C]//Proceedings of the AAS/AIAA Astrodynamics Specialist Conference. [S.l.]: AIAA, 2015.

[20] SULLIVAN J, KOENIG A, D'AMICO S. Improved maneuver-free approach to angles-only navigation for space rendezvous[C]//Proceedings of the 26th AAS/AIAA Space Flight Mechanics Meeting. [S.l.]: AIAA, 2016.

[21] WANG K, CHEN T, XU S. Relative navigation method based on dual line-of-sight measurement[J]. Acta Aeronautica et Astronautica Sinica, 2011, 32(6): 1084-1091.

[22] BRUIJN F D, GILL E, HOW J. Comparative analysis of cartesian and curvilinear Clohessy-Wiltshire equations[J]. Journal of Aerospace Engineering, Sciences and Applications, 2011, 3(2): 1-15.

[23] GAIAS G, D'AMICO S, ARDAENS J S. Generalized multi-impulsive maneuvers for optimum spacecraft rendezvous in near-circular orbit[J]. International Journal of Space Science and Engineering, 2015, 3(1): 68-88.

[24] CHERNICK M, D'AMICO S. New closed-form solutions for optimal impulsive control of spacecraft relative motion[J]. Journal of Guidance, Control, and Dynamics, 2018, 41(2): 301-319.

[25] KOENIG A, GUFFANTI T, D'AMICO S. New state transition matrices for relative motion of spacecraft formations in perturbed orbits[C]//Proceedings of the AIAA/AAS Astrodynamics Specialist Conference. [S.l.]: AIAA, 2016.

[26] GAIAS G, ARDAENS J S, MONTENBRUCK O. Model of J_2 perturbed satellite relative motion with time-varying differential drag[J]. Celestial Mechanics and Dynamical Astronomy, 2015, 123(4): 411-433.

[27] BINGHAM B, GELLER D. Preliminary orbit determination for orbital rendezvous using Gauss method[C]//Proceedings of the AAS/AIAA Astrodynamics Specialist Conference. [S.l.]: AIAA, 2007.

[28] D'AMICO S. Autonomous formation flying in low earth orbit[D]. Delft, Netherlands: Delft University, 2010.

[29] GAIAS G, D'AMICO S, ARDAENS J S. Angles-only navigation to a non-cooperative satellite using relative orbital elements[J]. Journal of Guidance, Control, and Dynamics, 2014, 37(2): 439-451.

[30] CRASSIDIS J L, JUNKINS J L. Optimal estimation of dynamic systems[M]. London, UK: CRC Press, 2001.

[31] MYERS K, TAPLEY B. Adaptive sequential estima-

tion with unknown noise statistics[J]. IEEE Transactions on Automatic Control, 1976, 21(4): 520-523.

[32] ZHANG S Q. Space rendezvous and docking measurement technology and engineering application[M]. Beijing, China: China Aerospace Publishing House, 2005: 396-397.

Acknowledgement This work was supported by the China Aerospace Science and Technology Corporation Eighth Research Institute Industry-University-Research Cooperation Fund (No.SAST 2020-019).

Authors Dr. **DU Ronghua** received the B.S. degree in mechanical engineering from the School of Mechanical Engineering, Nanjing University of Science and Technology, Nanjing, China, in 2017. He is currently pursuing the Ph.D. degree in mechanical engineering from the School of Mechanical Engineering, Nanjing University of Science and Technology, Nanjing, China. His research interests include satellite attitude determination, vision-based relative navigation, guidance navigation and control, and angles-only relative navigation.

Prof. **LIAO Wenhe** received the B.S. degree in aerospace manufacturing engineering from the College of Mechanical and Electrical Engineering, Nanjing University of Aeronautics and Astronautics, Nanjing, China, in 1990 and Ph.D. degree in aerospace manufacturing engineering from the College of Mechanical and Electrical Engineering, Nanjing University of Aeronautics and Astronautics, Nanjing, China, in 1996. He is currently the vice president of the Nanjing University of Science and Technology, Nanjing, China. He is also the director of the Micro Satellite Research Centre and a professor with the College of Mechanical Engineering, Nanjing University of Science and Technology, Nanjing, China. His research interests include satellite system design and high-end equipment design.

Author contributions Dr. **DU Ronghua** designed the conceptualization and methodology. Prof. **LIAO Wenhe** helped design the methodology and reviewed the manuscript. Prof. **ZHANG Xiang** contributed to perform the analysis and discuss the background of the study. All authors commented on the manuscript draft and approved the submission.

Competing interests The authors declare no competing interests.

(Production Editor: ZHANG Bei)

基于非线性动力学法的航天器非合作交会仅测角导航

杜荣华，廖文和，张　翔

(南京理工大学机械工程学院，南京 210094，中国)

摘要：针对航天器非合作交会中的相对导航问题，提出了一种基于非线性动力学法的仅测角导航的新架构。该方法没有通过轨道或姿态机动来解决仅测角导航可观性较差的问题，而是通过捕捉系统在相对运动演变中的非线性来提高仅测角导航系统的可观性。首先，介绍了3种相对动力学模型及其对应的视线(Line-of-sight, LoS)测量方程，包括直线状态相对动力学、曲线状态相对动力学和相对轨道根数(Relative orbital elements, ROE)状态相对动力学模型。然后，引入了基于Gramian矩阵的可观性分析理论用于确定哪个相对动力学模型可以最大化仅测角导航的可观性。接着，介绍了一种自适应扩展Kalman滤波方案，用以解决非线性动力学法中仅测角导航滤波器对测量噪声非常敏感的问题。最后，通过数值仿真的手段对提出的仅测角导航滤波架构进行了测试和验证，证明了通过改进相对动力学和LoS测量模型，无机动的仅测角导航是完全可行的。

关键词：仅测角导航；非线性动力学；可观性分析；非合作交会；自适应Kalman滤波